Design of the star-shaped tip pruning device for broad-leaved tall-stemmed crops based on UAV payload and optimization of its operation parameters

Lianhao Li[1], Guozhen Ma[1], Xiaoyong Liu[1], Chenhui Zhu[1], Qiantao Sun[2], Weihua Qin[3*], Zhimin Jia[4], Zhijing Wen[4]

(1. *College of Mechanical and Electrical Engineering, Henan Agricultural University, Zhengzhou 450002, China*;
2. *Henan Academy of Agricultural Sciences Changyuan Branch, Changyuan 453400, China*;
3. *Henan Province Tobacco Company Sanmenxia City Company, Sanmenxia 472099, Henan, China*;
4. *School of Intelligent Mechatronics Engineering, Zhongyuan University of Technology, Zhengzhou 450002, China*)

Abstract: In mountainous and hilly areas, the tip pruning and flower removal operations for broad-leaved tall-stemmed plants are labor-intensive tasks. It is vital for reducing labor costs of broad-leaved tall-stemmed plants to mechanize this operation. To deal with this problem, a tip pruning device which utilizes an unmanned aerial vehicle (UAV) as a carrier to autonomously locate and target broad-leaved tall-stemmed plants is designed in this paper. Firstly, the primary mechanical properties of broad-leaved tall-stemmed plants at full bloom are explored, laying the groundwork for subsequent device design (tobacco is the primary crop studied). Then, the shape and key parameters of the cutting tool for the UAV-mounted tip pruning device, as well as the key parameters of the rhomboid retractable component, are defined based on dynamic analysis, which satisfy demand for the tip pruning device operation. Finally, an adaptive control system for the tip pruning device is developed. The optimization experiments of operational parameters indicate that when the UAV travels at a speed of 0.8 m/s and the tip pruning blade rotates at 1200 r/min, the tip pruning integrity rate exceeds 98.2%, which shows excellent operational performance and the ability to meet actual production demands. This study has significant implications for improving the mechanization and intelligence of tip pruning and flower picking operations in high stem plants.

Keywords: broad-leaved tall-stemmed plants, tip pruning device, star-type, terminal bud, unmanned aerial vehicle
DOI: 10.25165/j.ijabe.20261901.9863

Citation: Li L H, Ma G Z, Liu X Y, Zhu C H, Sun Q T, Qin W H, et al. Design of the star-shaped tip pruning device for broad-leaved tall-stemmed crops based on UAV payload and optimization of its operation parameters. Int J Agric & Biol Eng, 2026; 19(1): 108–119.

1 Introduction

As a major broad-leaved tall-stemmed plants-producing country, China regards broad-leaved tall-stemmed plants as an important economic crop, with its planting area and yield ranking first in the world (tobacco is its primary representative crop). Broad-leaved tall-stemmed plant taxes provide strong support and assurance for the national fiscal revenue, holding a very significant position in national production[1,2].

In the broad-leaved tall-stemmed plants production process, the tip pruning operation is one of the key steps in the field production process, having a critical impact on broad-leaved tall-stemmed plants production. Failure to top and suppress buds in broad-leaved tall-stemmed plants can lead to a decrease in the yield and quality of broad-leaved tall-stemmed plants leaves, increase the risk of disease, and affect the normal growth of broad-leaved tall-stemmed plants, among other issues[3-6].

At present, the broad-leaved tall-stemmed plants tip pruning process is predominantly carried out manually, which is labor-intensive and costly. With societal development, the mechanization level of broad-leaved tall-stemmed plants tip pruning operations is also continuously improving[7-11]. Numerous scholars both domestically and internationally have conducted research in this area. For instance, Wu et al.[12] have designed a self-propelled clamping intelligent broad-leaved tall-stemmed plants tip pruning device, Liu et al.[13] have developed a dual-row intelligent broad-leaved tall-stem plants tip pruning device, and Han et al.[14] have created a lightweight backpack-style broad-leaved tall-stemmed plants tip pruning device. The above-mentioned tip pruning devices had certain drawbacks. First, its large size is incompatible with the actual conditions of tobacco fields in China, leading to poor adaptability to diverse terrains and field plots as well as limited application scenarios. Second, it lacks operational flexibility and adaptability to farming seasons. In addition, it is prone to damage tobacco plants, which increases the difficulty of controlling the operation quality. Additionally, Canadian Patent (No. 1026565) describes a tip pruning device used in conjunction with a broad-leaved tall-stemmed plants harvester. Raymond et al. have developed a mechanical device that performs tip pruning and applies bud suppressants simultaneously. These achievements have certain guiding significance for the mechanized tip pruning

Received date: 2025-04-22 **Accepted date:** 2026-01-15
Biographies: Lianhao Li, PhD, Associate Professor, research interest: intelligent agricultural machinery equipment, Email: lianhao8022@126.com; **Guozhen Ma**, MS, research interest: agricultural mechanization engineering, Email: 15939692053@163.com; **Xiaoyong Liu**, Engineer, research interest: intelligent agricultural machinery equipment, Email: liuxiaoyong74@sina.com; **Chenhui Zhu**, PhD, Lecturer, research interest: intelligent agricultural equipment, Email: zhuchenhui@henau.edu.cn; **Qiantao Sun**, Engineer, research interest: intelligent agricultural machinery equipment, Email: 1640696029@qq.com; **Zhimin Jia**, MS, research interest: intelligent agricultural machinery equipment, Email: 1022727734@qq.com; **Zhijing Wen**, MS, research interest: intelligent agricultural machinery equipment, Email: yunyunxxy@163.com.
***Corresponding author: Weihua Qin**, Agronomist, research interest: agricultural mechanization engineering. Xiaoshan East Road, Hubin District, Sanmenxia 472000, Henan, China. Tel: +86-18339885598, Email: qinweihua@126.com.

operations in broad-leaved tall-stemmed plants cultivation.

The aforementioned research achievements demonstrated excellent operational effectiveness in open plains areas. However, they show poor applicability in mountainous and hilly regions, primarily due to low operational efficiency and the inability to execute effective turns. At present, the majority of broad-leaved tall-stemmed plants cultivation in China is conducted on sloped terraces, with over 70% of broad-leaved tall-stemmed plants fields distributed across mountainous and hilly areas. Additionally, the varying positions of broad-leaved tall-stemmed plants flowers result in poor tip pruning outcomes. Therefore, the development of a broad-leaved tall-stemmed plants tip pruning device that is suitable for mountainous and hilly regions, characterized by its light weight and high flexibility, has become an urgent problem to be addressed.

Therefore, this paper develops a star-type broad-leaved tall-stemmed plants tip pruning device based on UAV payload, primarily composed of a star-type tip pruning mechanism, a rhomboid retractable mechanism, and an adaptive control system. Utilizing an existing UAV as a carrier, it can autonomously locate broad-leaved tall-stemmed plants flowers, effectively resolving the aforementioned problems. This research holds significant importance for effectively reducing the labor intensity and cost of broad-leaved tall-stemmed plants tip pruning operations and enhancing the level of agricultural machinery intelligence in our country.

2 Structure design and working principles of overall machine

2.1 Structure design

The broad-leaved tall-stemmed plants tip pruning device mainly consists of the UAV payload platform, a driving power source, a landing gear, a star-type tip pruning cutter, a diamond-shaped retractable mechanism, and an adaptive control system (see Figure 1). Bearings are installed at the junctions of the diamond structure to reduce friction among various components during the tip pruning operation. The main operational parameters are listed in Table 1.

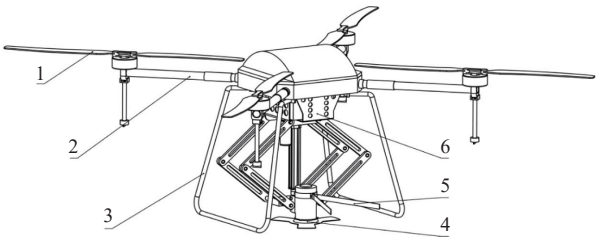

1. Wings of an unmanned aerial vehicle (UAV) 2. Rotor support arm 3. Landing gear 4. Star-type tip pruning cutter 5. Grain lifter 6. Drive power supply

Figure 1 Star-type broad-leaved tall-stemmed plants tip pruning device based on UAV payload

Table 1 Main operating parameters

Total mass/kg	Flight speed/ m·s^{-1}	Operating altitude/ m	Endurance time/min
25	0-15	2-6	10-20

2.2 Working principle

Firstly, the basic height of the broad-leaved tall-stemmed plants needs to be determined. Then the star-type broad-leaved tall-stemmed plants tip pruning device was operated based on the UAV payload to move it to the top of the broad-leaved tall-stemmed plants (reaching the basic height 1). The adaptive system captures the position of the broad-leaved tall-stemmed plants and autonomously adjusts the diamond-shaped retractable component to position the star-type cutter at the tip pruning point (approximately 30-50 cm above the plant apex[15]). The tip pruning device is activated, and as the UAV moves in the direction of tip pruning, the grain reel is used to gather the broad-leaved tall-stemmed plants into the range of the star-type cutter. Then, the star-type cutter is rotated to perform the tip pruning. After completing the tip pruning operation, the tip pruning device is retracted into the landing gear by driving the diamond-shaped retractable mechanism with an electric push rod. The UAV safely returns and lands, ultimately completing the entire tip pruning process. The operation process is shown in Figure 2.

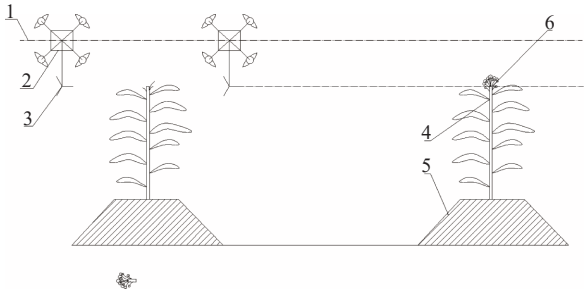

1. Basic flight altitude of the UAV 2. Multi-rotor unmanned aerial vehicle (UAV) 3. Star-type tip pruning blade 4. Broad-leaved tall-stemmed plants stalk 5. Broad-leaved tall-stemmed plants ridge 6. Broad-leaved tall-stemmed plants flower

Figure 2 Operation process

3 Design of key components and system

By analyzing the agronomic requirements, it is evident that the star-type tip pruning cutter, diamond-shaped retractable mechanism, and adaptive control system are the key components and systems of the star-type broad-leaved tall-stemmed plants tip pruning device based on the UAV payload.

3.1 Determination of the main mechanical properties of broad-leaved tall-stemmed plants flowers

Qinyan-96, widely cultivated in Henan Province, was selected as the experimental material. The stem samples of broad-leaved experimental material were collected from a position approximately 300 mm below the apex during the bud stage of broad-leaved tall-stemmed plants growth. A total of 200 plants were sampled, with an average moisture content of about 89.9%. The main mechanical properties of the tip pruning break point and the broad-leaved tall-stemmed plants stem were measured to provide technical references for the structural parameter design of the star-type tip pruning mechanism.

Based on the principle of the wood moisture content determination method specified in GB/T 1927.4-2021, it is considered that the mass lost by the test sample during the drying process is the moisture content of the sample.

The calculation equation for moisture content is as follows:

$$N = \frac{M - m}{M} \times 100\% \tag{1}$$

where, N is moisture content, %; M is initial mass, g; m is oven-dried mass, g.

The test results are listed in Table 2. The measuring instruments mainly include: WDE-1E electronic universal testing machine, digital display Vernier caliper (with an accuracy of

0.02 mm), tape measure, cutting tool, etc. When measuring the shear force at the tip pruning break point, the loading speed was set to 20 mm/min. After the shear test, the maximum shear force was read and recorded. For the bending test of the broad-leaved tall-stemmed plants stem, a 100 mm section of the stem was taken, and the three-point bending measurement method was used with a loading speed of 10 mm/min. The shear modulus of the broad-leaved tall-stemmed plants stem was calculated by measuring the relationship between pressure and displacement[16]. The test results for the mechanical properties of the broad-leaved tall-stemmed plants are listed in Table 3.

Table 2 Determination results of moisture content in tobacco stalks

Group No.	Sample wet weight/g	Oven-dried mass/g	Moisture content/%
1	45.62	4.61	89.89
2	52.35	5.28	89.92
3	48.90	4.93	89.89
4	56.78	5.72	89.91
5	41.25	4.15	89.88
6	50.10	5.05	89.90
Average	49.17	4.96	89.90

Table 3 Main mechanical properties of tobacco flower samples

Serial No.	Sample diameter/m	Shear force at the shear point/N	Shear modulus of firework stem/MPa
1	11-15	48-68	15-25

3.2 Star-shaped cutter

3.2.1 Determination of cutter shape

The tip pruning mechanism for broad-leaved tall-stemmed plants must take into account various factors, such as the mechanical properties of broad-leaved tall-stemmed plants stems, growth characteristics, and operational environment[17].

To appropriately select the shape of the cutting tool (Figure 3), the concept of the cutting completeness rate of broad-leaved tall-stemmed plants is introduced. The cutting completeness rate refers to the qualification level of broad-leaved tall-stemmed plants after tip pruning. According to the basic requirements of tip pruning, a cut is considered effective only if the following two conditions are simultaneously met during the tip pruning process:

(1) The broad-leaved tall-stemmed plants are completely cut by the cutting tool during the tip pruning process.

(2) After the broad-leaved tall-stemmed plants are completely cut by the cutting tool during the tip pruning process, the flatness of the cut surface is relatively even.

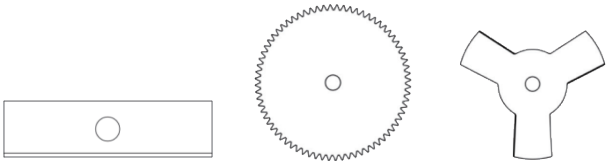

a. Straight-line cutter b. Triangular star-shaped cutter c. Circular cutter

Figure 3 Common tip pruning cutters

Therefore, the cutting completeness rate is defined as:

$$K = \frac{K_1}{K_2} \times 100\% \quad (2)$$

where, K is the cutting completeness rate of the broad-leaved tall-stemmed plants, %; K_1 is the number of effectively cut broad-leaved tall-stemmed plants; and K_2 is the total number of broad-leaved tall-stemmed plants tested for cutting.

According to the requirements for tip pruning broad-leaved tall-stemmed plants, the effective tip pruning rate must exceed 97%[18]. Therefore, during the broad-leaved tall-stemmed plants tip pruning experiment, the probability of meeting the cutting requirements for broad-leaved tall-stemmed plants was recorded. The test results are listed in Table 4, and the effect is shown in Figure 4.

Table 4 Effective cutting completeness rate of broad-leaved tall-stemmed plants with different cutting tools

Cutting tool	Cutting completeness rate/%	Qualification probability
Straight-line type	89	0.88
Toothed type	91	0.90
Star-shaped Type	99	0.98

a. Cutting with straight-blade tool b. Cutting with circular tool c. Cutting with star-shaped tool

Figure 4 Cutting effects of three types of tools

From Table 4, it can be observed that, according to the requirements for tip pruning broad-leaved tall-stemmed plants, the qualification probability of the star-shaped cutting tool is higher than that of the toothed type, which in turn is higher than that of the straight-line type. This is primarily due to the deformation of the cutting tools during the cutting process, which leads to a reduction in the effective cutting rate.

3.2.2 Analysis of the broad-leaved tall-stemmed plants cutting process using a cutting tool

The cutting edge of a star-shaped tool primarily consists of the main cutting edge, rake face, main flank face, tool tip, auxiliary cutting edge, and auxiliary flank face (as shown in Figure 5). The main cutting edge is the intersection line between the rake face and the main flank face of the tool. The main flank face is the surface of the tool that interacts with and faces the machined surface of the work piece. The tool tip is the intersection point of the main cutting edge and the auxiliary cutting edge. The auxiliary flank face is the surface of the tool that interacts with and faces the already machined surface of the work piece. The auxiliary cutting edge is the intersection line between the rake face and the auxiliary flank face. The rake face is the surface of the tool over which the chip flows.

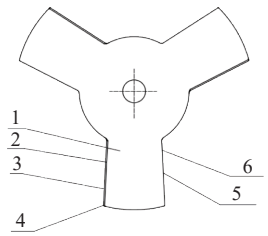

1. Main cutting edge 2. Rake face 3. Main flank face 4. Tool tip 5. Auxiliary cutting edge 6. Auxiliary flank face

Figure 5 Composition of the tool tooth cutting edge

(1) Analysis of broad-leaved tall-stemmed plants cutting path

When broad-leaved tall-stemmed plants flowers are being cut,

the star-shaped cutting tool rotates at a constant angular velocity ω as the drive shaft turns, while simultaneously moving at a constant speed V_1 in a straight line towards the broad-leaved tall-stemmed plants flower. To study the motion trajectory of the star-shaped cutting tool, a point M is selected at the tip of the blade. The motion of point M can be considered as a combination of circular motion with angular velocity ω and linear motion with speed V_1. The resulting trajectory of point M at the blade tip is illustrated in Figure 6.

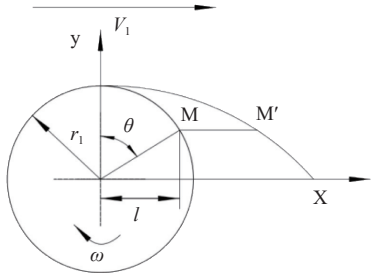

Figure 6 Diagram of the tool cutting motion trajectory

The equation for the motion trajectory of the M point tool cutting is established as follows:

$$\begin{cases} x_M = V_1 t + r_1 \sin\theta \\ y_M = r_1 \cos\theta \\ \theta = \omega t \end{cases} \tag{3}$$

where, r_1 is the radius of the star-shaped cutting tool, m; ω is the angular velocity of the star-shaped cutting tool, rad/s; V_1 is the forward speed of the star-shaped cutting tool, m/s; x_M is the displacement of the blade tip M in the x-direction, m; y_M is the displacement of the blade tip M in the y-direction, m; θ is the motion angle of the blade tip M; and t is the motion time of the blade tip M, s.

By differentiating the displacement in the x-direction and the displacement in the y-direction of the cutting point on the broad-leaved tall-stemmed plants stalk, the velocity of the cutting point on the broad-leaved tall-stemmed plants stalk is obtained as:

$$\begin{aligned} V_X &= \frac{d_{x_M}}{d_t} = V_1 + \omega r_1 \cos\omega t \\ V_y &= \frac{d_{y_M}}{d_t} = -\omega r_1 \sin\omega t \end{aligned} \tag{4}$$

The velocity of the cutting point M is synthesized from the velocity vectors in the x-direction and the y-direction, that is, the square of the velocity of the cutting point M equals the sum of the squares of the velocities in the x-direction and the y-direction:

$$V_M^2 = V_x^2 + V_y^2 \tag{5}$$

Taking the square root of the above equation yields the velocity of the cutting point M:

$$V_M = \sqrt{V_1^2 + \omega^2 r_1^2 + 2\omega r_1 \cos\omega t} \tag{6}$$

where, V_x is the velocity of the knife edge M in x-direction, m/s; V_y is the velocity of the knife edge M in the y-direction, m/s; V_M is the vector velocity of the gear tip M, m/s.

(2) Stress analysis of broad-leaved tall-stemmed plants stalk cutting

When cutting broad-leaved tall-stemmed plants flowers, it can be simplified as a cantilever beam structure where the bottom end does not experience displacement, and the top end can generate axial and radial forces. During the cutting process, the stalk of the broad-leaved tall-stemmed plants flowers bends under the cutting force, resulting in a nearly circular shape at the cutting edge. For ease of analysis, the cross-section of the cut is considered circular, as shown in Figure 7. The forward speed of the star-shaped cutter is V_1, and the cutting force can be decomposed into a normal sliding force F_1, a radial force F_2, and an axial force F_3. Among these, the normal sliding force F_1 is the primary factor affecting the cutting action of the circular blade. The radial force F_2 mainly arises from the reaction force exerted by the broad-leaved tall-stemmed plants on the star-shaped cutter, while the axial force F_3 is primarily generated by the impact and compression of the broad-leaved tall-stemmed plants flowers on the cutter, directed perpendicular to the surface of the cutter.

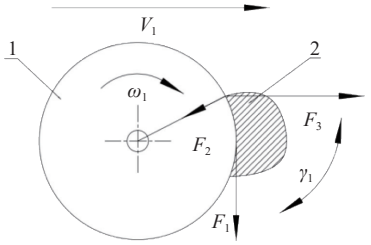

1. Tip pruning blade 2. Cross-section of the broad-leaved tall-stemmed plants top stalk

Figure 7 Diagram of force analysis for tip pruning

(3) The fundamental condition for ensuring a complete cutting of the broad-leaved tall-stemmed plants without omission

Missed cutting presents the phenomenon during the broad-leaved tall-stemmed plants cutting process where, due to insufficient cutting by the cutting tool, the plant is directly pushed over by the feeding motion of the tip pruning device, resulting in the plant not being cut or even breaking. The occurrence of missed cutting significantly affects the effectiveness of tip pruning. Therefore, the star-shaped cutter is simplified to a model with only three pairs of adjacent cutting teeth (taking a pair of teeth as an example), with the parameters as shown in Figure 8. BC represents the blade surface of any cutter, AD denotes the blade surface of an adjacent star-shaped cutter, r_1 is the radius of the blade, R_1 is the length of the star-shaped cutter's surface, δ is the blade inclination angle of the star-shaped cutter, σ is the inter-blade angle of the star-shaped cutter, θ is the central angle (0°) between the top and root of the star-shaped cutter's blade relative to the axis of the blade, ω is the angular velocity of the star-shaped cutter, and V_x is the forward speed of the multi-rotor drone.

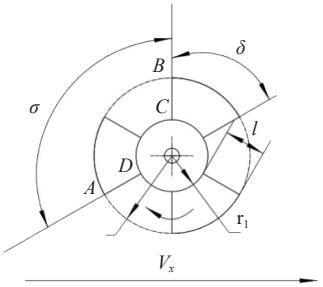

Figure 8 Cutter parameters

During the tip pruning operation, the star-shaped cutter performs uniform rotational and linear feeding motions. To calculate the motion equation of the cutter's tip, the center of the star-shaped cutter is set as the displacement origin, with x-direction of the drone's feed as the positive axis direction. The star-shaped cutter rotates clockwise for the cutting motion, yielding the motion

equation for any tip point B of the star-shaped cutter:

$$\begin{cases} x_B = V_x t + r_2 \sin\omega t \cos\phi \\ y_B = r_2 \cos\omega t \\ z_B = -R_2 \sin\omega t \sin\phi \end{cases} \tag{7}$$

where, r_1 is the radius of the star-shaped cutter, m; r_1 is the radius of the cutting edge, m; t is the cutting time of the blade edge, s; V_x is the forward speed of the drone.

Similarly, the motion equation for the root point of the blade tooth is:

$$\begin{cases} x_C = V_x t + r_2 \sin(\omega t + \theta) \cos\phi \\ y_C = r_1 \cos(\omega t + \theta) \\ z_C = -r_1 \sin(\omega t + \theta) \sin\phi \end{cases} \tag{8}$$

Analysis of the broad-leaved tall-stemmed plants stalk cutting process reveals that the condition for the star-shaped cutter to avoid missed cuts is as follows: the shadow area covered by the sweeping trajectory of any blade tooth of the cutting blade must have no gaps with the shadow area covered by the sweeping trajectory of the next adjacent blade tooth. Consequently, it is necessary to calculate the motion trajectory of the next adjacent blade tooth.

The motion equation for the point A of the next adjacent blade tooth tip is:

$$\begin{cases} x_A = V_x t + r_2 \sin(\omega t - \sigma) \cos\phi \\ y_A = r_2 \cos(\omega t - \sigma) \\ z_A = -r_2 \sin(\omega t - \sigma) \sin\phi \end{cases} \tag{9}$$

The motion equation for the tip D of the next adjacent blade tooth is:

$$\begin{cases} x_D = V_x t + r_1 \sin(\omega t - \sigma + \theta) \cos\phi \\ y_D = r_1 \cos(\omega t - \sigma + \theta) \\ z_D = -r_1 \sin(\omega t - \sigma + \theta) \sin\phi \end{cases} \tag{10}$$

where, σ is the inter-blade angle of the cutter teeth, (°); θ is the central angle between the top and root of the blade relative to the axis of the blade, (°).

The inter-blade angle of the cutter teeth:

$$\sigma = \frac{2\pi}{Z} \tag{11}$$

where, Z is the number of cutter teeth.

When the swept area formed by the cutting trajectories of any blade tip B and tooth root C of a star-shaped cutting tool and the adjacent rear blade's tooth tip A and tooth root D has no gaps, in the xoy plane, the coordinates of any blade tip B at time t and the adjacent blade tip A at time $t+\Delta t$ have the following relationship:

$$\begin{cases} y_B(t) = y_A(t + \Delta t) \\ x_{AB} = x_A(t) - x_B(t) \end{cases} \tag{12}$$

Thus, the distance between the adjacent two blade edges cutting the specimen is written as:

$$x_{AB} = x_A(t) - x_B(t) = V_1 \Delta t + r_1 \sin(\omega t - \sigma) \tag{13}$$

Differentiate Equation (11) to solve:

$$\frac{dx_{AB}}{d_t} = 0 \tag{14}$$

$$\frac{d^2 x_{AB}}{dt^2} < 0 \tag{15}$$

By combining Equation (2) with Equation (14), the condition for ensuring no missed cuts during broad-leaved tall-stemmed plants stalk cutting is obtained:

$$V_1 \le \frac{l \cos\delta \omega Z}{2\pi} \tag{16}$$

where, l represents the length of the blade back edge, m. Therefore, to prevent the occurrence of missed cuts during the broad-leaved tall-stemmed plants stalk cutting process, the feed speed should satisfy the condition specified in Equation (15). Based on this, the maximum feed speed for the broad-leaved tall-stemmed plants stalk cutting test bench can be calculated (V_1≤1.11 m/s).

3.2.3 Structure and parameters of the star-shaped cutting tool

The star-shaped cutting tool serves as the direct component for linear cutting operations in cutting tasks. Its selection is primarily based on three parameters: outer diameter (D), mounting hole diameter (d), and blade thickness (C), as illustrated in Figure 9.

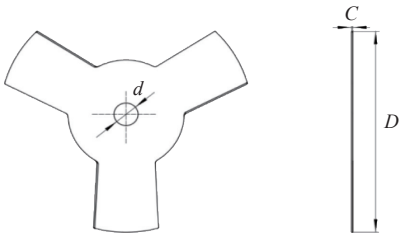

Figure 9 Star-shaped cutting tool

Currently, star-shaped cutting tools suitable for tobacco flower cutting in the domestic market mainly include carbide steel blades and manganese steel blades. For cutting high-hardness materials (such as metal or stone), carbide steel blades are often preferred, requiring high equipment stability, specialized cutting machines, and strict operational standards. Manganese steel blades, on the other hand, are commonly used for high-speed cutting, capable of withstanding significant loads and vibrations. They are easy to manufacture, highly adaptable, and frequently employed in woodworking and plastic cutting. For this test bench, the star-shaped cutting tool is made of 65 Mn steel.

The outer diameter of the star-shaped cutting tool is generally determined based on the performance requirements and dimensions of the broad-leaved tall-stemmed plants stalk equipment. Star-shaped tools with smaller outer diameters typically achieve lower maximum rotational speeds and are suitable for low-speed cutting. Conversely, tools with excessively large outer diameters demand higher overall mechanical performance and generate significant noise during operation. Given that broad-leaved tall-stemmed plants stalks are relatively thin, the outer diameter of the star-shaped tool should not be excessively large to avoid wasting performance. In China, the outer diameters of such tools typically range from 110~1800 mm. Domestically produced blades are usually designed in increments of 50 mm. Taking these factors into account, a manganese steel tool with an outer diameter of 200~300 mm is selected.[19]

The thickness of the disc blade is proportional to the square root of the blade diameter, which can be expressed as:

$$C = K\sqrt{D} \tag{17}$$

where, D represents the blade diameter in mm; K is the thickness coefficient. When D ranges from 100-650 mm, K is taken as 0.065; when D ranges from 650-1200 mm, K is taken as 0.075; and when D ranges from 1200-1800 mm, K is taken as 0.11, with an average value of 0.07. According to cutting theory, a smaller blade thickness indicates better cutting performance. However, in practical working

conditions, excessively thin blades can generate stronger vibrations during cutting, and in severe cases, may lead to chipping or breakage.

The star-shaped blade is similar to a circular blade, and determining the aperture is relatively straightforward. Currently, for standard components designed domestically, the aperture for outer diameters of 120 mm and below is mostly 20 mm; for diameters between 20-230 mm, it is mostly 25.4 mm; and for diameters above 250 mm[20], it is mostly 30 mm. Some imported equipment may also feature a 15.875 mm aperture. This design adopts the domestic standard aperture, utilizing a circular blade with a 25 mm aperture. Additionally, it ensures that the blades replaced during the experiment are of the same aperture, making the process convenient and efficient.

In the blade design process, the greater the number of teeth, the more cutting edges engage per unit time, resulting in better cutting performance. However, an increase in the number of teeth also raises the cost of the blade. Moreover, excessively dense teeth can reduce the chip clearance between teeth, leading to an increase in blade temperature. Additionally, improper coordination between the teeth and the feed rate can exacerbate edge wear, affecting the blade's service life. For this experimental design, a 3-tooth star-shaped blade is adopted, which can avoid the aforementioned problems.

The primary angular parameters of the star-shaped blade teeth include the rake angle α, clearance angle β, and wedge angle γ. The rake angle is the angle between the front face of the blade and the base plane, the clearance angle is the angle between the rear face of the blade and the cutting plane, and the wedge angle is the angle between the front face and the rear face of the blade. The cutting plane of the star-shaped tool is illustrated in Figure 10. A larger rake angle facilitates easier cutting, while a larger clearance angle reduces friction between the blade teeth and the machined surface. The wedge angle, derived from the first two angles, plays a role in maintaining the strength, durability, and heat dissipation of the blade teeth.

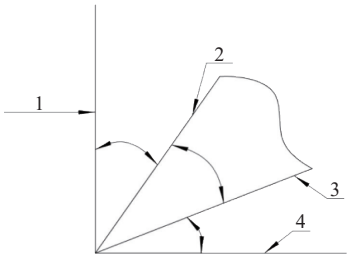

1. Base plane 2. Rake face 3. Flank face 4. Cutting plane

Figure 10 Cutting plane of the star-shaped tool

Common blade tooth profiles include alternate top bevel, flat top, trapezoidal flat top, reverse taper, and dovetail teeth, among others[21]. Reverse taper teeth lack sufficient strength and result in rough cutting surfaces; flat top teeth generate significant friction, leading to slower speeds, heat buildup, and poor chip removal, making them suitable for flat-top surface treatments. Trapezoidal flat top teeth involve complex manufacturing processes and are more expensive, but they reduce surface chipping during cutting and are suitable for various single or double-faced artificial boards and fireproof boards. Alternate top bevel teeth are the most widely used, offering high cutting efficiency, relatively simple sharpening, and smooth, flat cutting surfaces, making them suitable for broad-leaved tall-stemmed plants stalk cutting. This design adopts alternate top bevel teeth.

The final selected parameters of the star-shaped cutting tool are listed in Table 5.

Table 5 Specification parameters of the circular blade

Material	Diameter/ mm	Aperture/ mm	Number of teeth	Tooth width/mm	Thickness/ mm	Tooth profile
65 Mn	260	25	3	136	1-1.5	Trapezoidal tooth

3.3 Diamond-shaped retraction and extension mechanism

3.3.1 Structural design

In response to the need for adjusting the position of the star-shaped tip pruning cutter in real time to accommodate the location of broad-leaved tall-stemmed plants during the tip pruning operation, a diamond-shaped retraction and extension mechanism was designed[22]. This mechanism autonomously responds to the positional deviations determined by the adaptive control system, as illustrated in Figure 11. Located within the landing gear, and to ensure the safe takeoff and landing of the UAV's payload platform, the four-bar linkage dimensions were designed to be L_1=225 mm, considering the structural layout of the landing gear itself. Considering that the broad-leaved tall-stemmed plants tip pruning device is based on an existing UAV as the airborne platform, and without altering the overall structure of the existing UAV, the connection dimensions for the upper and lower platforms were designed to be M_1=M_2=125 mm for ease of installation and fixation of the diamond-shaped retraction and extension mechanism. Flight tests of the UAV have shown that the above design parameters meet the operational requirements for takeoff, landing, and installation fixation.

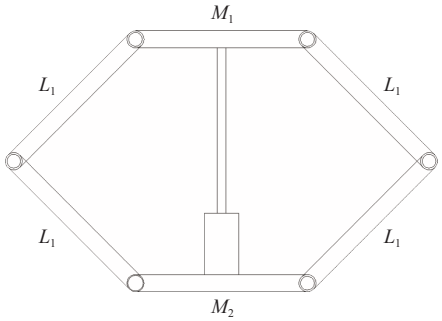

Figure 11 Diamond-shaped retraction and extension mechanism

To ensure the operational stability of the diamond-shaped retraction and extension mechanism, its degrees of freedom were calculated (considering constraints):

$$f = 3\times3 - 2\times4 = 1 \tag{18}$$

As can be seen from Equation (18), the degree of freedom of this structure is 1, which therefore satisfies the usage requirements.

3.3.2 Material selection

(1) Material property settings for the diamond-shaped retraction and extension mechanism

The retraction and extension mechanism assembly model, established in UG, was imported into the ADAMS analysis software to apply connection constraints, thereby creating a kinematic analysis model of the retraction and extension mechanism based on Adams, as shown in Figure 12. Given the low payload of the UAV itself and considering the need for lightweight onboard equipment, the material properties of the diamond-shaped retraction and extension mechanism and the electric actuator were set to aluminum alloy (Aluminum Alloy), with a density of 2770 kg/m^3, an elastic modulus of 7.17×10^{10} N·m, and a Poisson's ratio of 0.33. The

material properties of other components were set to structural steel (Structural Steel). Adams automatically calculated the mass of each component and the moment of inertia around the coordinate axes[22-25].

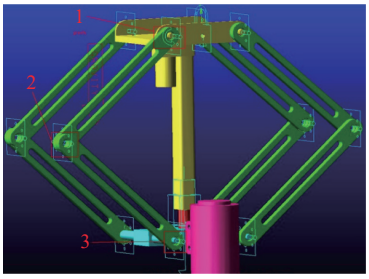

1.Joint 1; 2.Joint 2; 3.Joint 3

Figure 12 Simulation image

(2) Drive parameter settings and simulation result analysis

From the above analysis, it is understood that the diamond-shaped retraction and extension mechanism is primarily driven by an electric actuator. To ensure the flight stability of the UAV, the speed of the electric actuator should not be too high during operation, as excessive speed could cause an imbalance in the UAV's center of gravity, affecting flight safety. Based on field tests, the optimal speed for the electric actuator was determined to be 20 mm/s, at which the UAV operates quite well. At this constant speed, the actuator moves downward, reaching its maximum stroke (160 mm) from 0 s to 6 s. After staying at the lowest position for 6 seconds, it begins to move upward at a constant speed from the 12 s, retracting to its maximum stroke (160 mm) by the 19 s. The driving function is set as follows: step (time, 0, 0, 6, -160) + step (time, 6, 0, 12, 0) + step (time, 12, 0, 19, 160), and the total simulation time is set to 20 s, with the number of simulation steps set to 400. The average force results at key nodes during motion are shown in Figure 13.

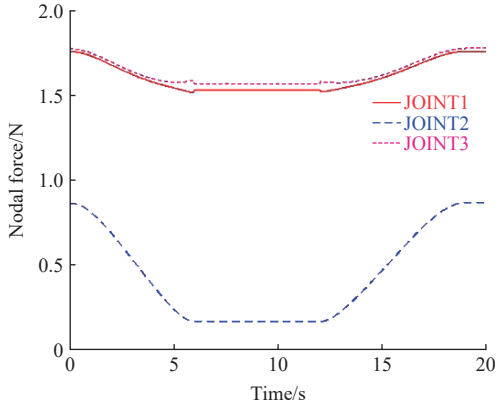

Figure 13 Relationship between the force of key nodes and time

Analyzing in conjunction with Figure 13, it can be observed that the forces at node 1 (Joint1) and node 3 (Joint3) remain relatively stable throughout the operation of the electric actuator. The maximum force at node 1 is 1.75 N, and the minimum force is 1.51 N. At node 3, the maximum force is 1.76 N, and the minimum force is 1.54 N. In contrast, the force at node 2 (Joint2) varies more significantly compared to nodes 1 and 3, with a maximum force of 3.5 N and a minimum force of 0.8 N. The analysis reveals the reasons: node 1 is primarily subjected to the dual effects of the upper platform's supporting force and the lower device's pulling force, node 3 mainly experiences the lower platform's pulling force and the connecting rod's supporting force, and node 2 is mainly influenced by the dual effects of the upper and lower platforms' pushing and pulling forces[22].

From the driving function, the simulation results of the relationship between the displacement and velocity of the lower platform and time are shown in Figure 14.

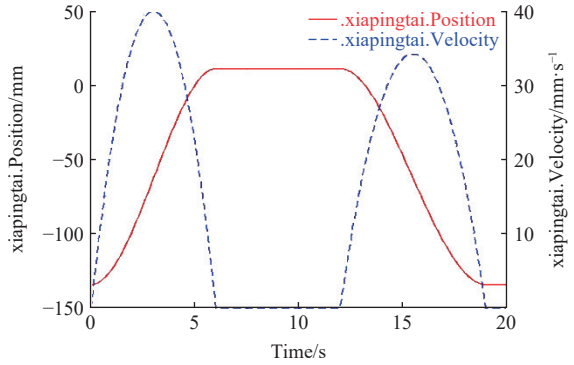

Figure 14 Curves of the displacement and velocity of the tip pruning platform versus time

From the analysis of Figure 14, it can be observed that the displacement (xiapingtai.Position) and velocity (xiapingtai. Velocity) curves of the lower platform remain relatively stable throughout the entire motion process, without significant fluctuations. The maximum velocity during the descent of the lower platform is 40 mm/s, while during the ascent, it is 34.8 mm/s. This difference is attributed to the gravitational force acting on the platform, which causes the maximum descent velocity to be greater than the maximum ascent velocity. Additionally, by correlating the actuator stroke with time, it is calculated that the average velocity during both the descent and ascent phases is 26.7 mm/s. Its relatively slow-motion speed adequately meets the requirements for operational stability[22].

3.4 Adaptive control system

3.4.1 Hardware composition

It is primarily composed of a high-definition camera, a controller, and an actuator, as illustrated in Figure 15.

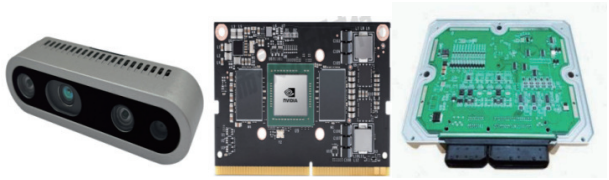

a. Binocular camera b. AI edge computing circuit board c. Controller

Figure 15 Hardware composition

3.4.2 Control system

To accommodate the varying height requirements for broad-leaved tall-stemmed plants tip pruning, an adaptive software control system for broad-leaved tall-stemmed plants positioning has been developed[26]. This system autonomously captures the position of the broad-leaved tall-stemmed plants and adjusts the position of the tip pruning device accordingly. The software control strategy is as follows:

1) Construct a multi-scale dataset of flue-cured broad-leaved tall-stemmed plants flowers and optimize the model for the task of small target detection.

2) After training, obtain a model for detecting flue-cured broad-leaved tall-stemmed plants flowers, compress it, and deploy it to edge computing devices.

3) Establish a target detection model based on YOLOv5. The specific steps are illustrated in Figure 16.

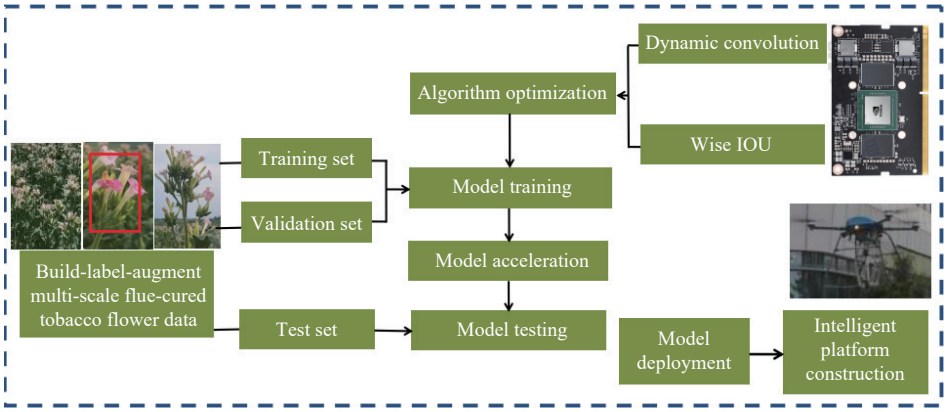

Figure 16 Target detection model

(1) Construction of broad-leaved tall-stemmed plants dataset

To establish a broad-leaved tall-stemmed plants dataset, the collection of broad-leaved tall-stemmed plants top image data was carried out in broad-leaved tall-stemmed plants-growing areas such as Nanyang, Xuchang, Pingdingshan, Luoyang, and Sanmenxia in Henan Province respectively. The cumulative number of images reached 8,000. The images are 1280×720 pixels in size and stored in JPG format. The collected images were screened, and finally 2800 broad-leaved tall-stemmed plants top images were selected. Data labeling was carried out, and a dataset was constructed, as shown in Figure 17.

(2) Identification model construction

Based on the YOLO model, a model for identifying the top of broad-leaved tall-stemmed plants is constructed. This model can meet the tip pruning requirements of broad-leaved tall-stemmed plants at different growth stages, including multiple categories such as immature (not yet reaching the tip pruning stage), early budding stage, budding stage, early flowering stage, full flowering stage, mature stage, and already topped. It satisfies the tip pruning needs of different growth periods under various planting patterns and also lays the foundation for subsequent research on the optimal mechanical tip pruning period. Currently, the model construction, training, and testing have been preliminarily completed, and it can be used to conduct experiments. In the later stage, it will be further optimized to improve the identification accuracy and speed.

(3) Model structure

A broad-leaved tall-stemmed plants top recognition model based on the YOLOv5 model is constructed. The Focus module is used in the backbone network for image slicing and sampling. Large-resolution images are finally normalized to the same size and fed into the neural network (as shown in Figure 18). Features are extracted by applying modules such as CBL, CSP, and SPP. After feature extraction, the features are sent to the intermediate layer. Different feature layers are combined with operations such as convolution for feature fusion. Feature maps of different scales are finally fused into three sizes and sent to the prediction part. Target prediction is finally achieved through convolution operations.

(4) Results of the adaptive test

Clustering analysis was performed on the categorical data to clarify the actual proportion of each category of data, as shown in Figure 19, as well as the size, distribution, and aspect ratio of the annotation boxes for each category, thus determining the optimal anchor box parameters. Preliminary tests demonstrate that the recognition rate exceeds 92% and the accuracy rate reaches 90%, which basically meets the production requirements, as illustrated in Figure 20.

Figure 17 Broad-leaved tall-stemmed plants dataset

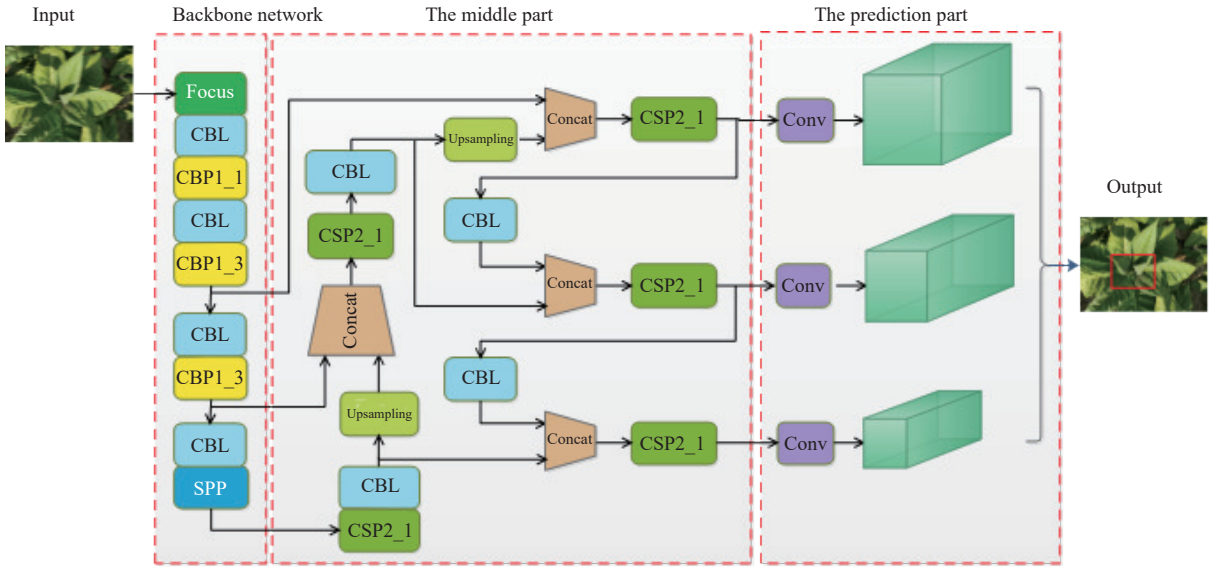

Figure 18 Neural network architecture

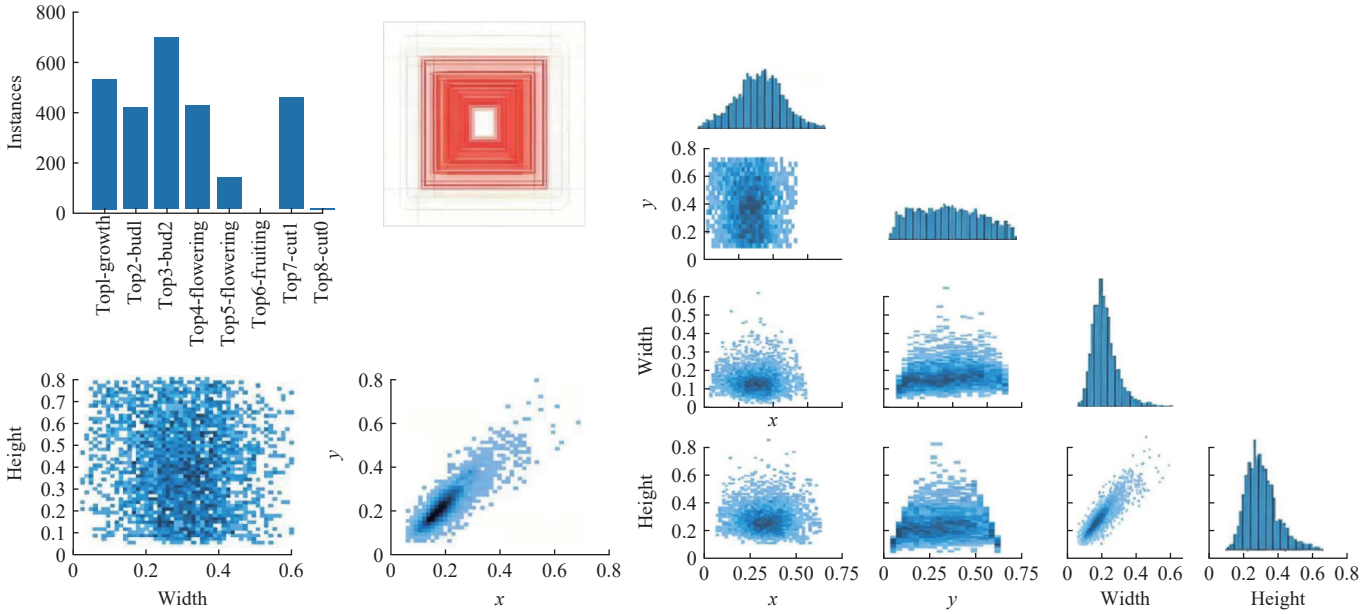

Figure 19 Cluster analysis of the collected data

Figure 20 Recognition effect

4 Optimization of working parameters

4.1 Orthogonal experimental design

To select the optimal working parameters, based on the previous single-factor tests, an orthogonal experiment was designed using Design-Expert.V8.0.6. A total of 17 groups of experiments were set up. To eliminate errors and ensure the accuracy of the experimental data, each group of experiments was repeated three times. The experimental factors and levels are listed in Table 6.

Table 6 Experimental design

Group	Blade rotation speed A/ r·min^{-1}	Forward speed B/m·s^{-1}	Broad-leaved tall-stemmed plants stem diameter C/mm
1	1000	0.6	10
2	1200	0.8	15
3	1400	1.0	20

4.2 Analysis and optimization of experimental results

The experimental results are listed in Table 7. The analysis shows that when the optimal combination of the experimental factors is a forward speed of 0.8 m/s and a blade rotation speed of 1200 r/min, the tip pruning rate is 99.1%.

4.3 Significance analysis of tip pruning efficiency

Through the analysis of the orthogonal experiment, the regression equation of the cleaning efficiency can be obtained as shown in Equation (19):

$$Y = 94.92 + 0.62A + 0.96B - 0.14C + 0.9AB + 1.75AC - 0.17BC + 0.78A^2 + 0.3B^2 - 0.7C^2 \quad (19)$$

where, Y is the tip pruning efficiency of broad-leaved tall-stemmed plants stems; A is the rotation speed of the blade; B is the forward speed; C is the diameter of the broad-leaved tall-stemmed plants stem.

Table 7 Experimental results

Serial No.	Blade rotation speed/r·min^{-1}	Forward speed/m/s	Broad-leaved tall-stemmed plants stem diameter/mm	Broad-leaved tall-stemmed plants stem tip pruning rate/%
1	1000	0.60	15.00	95.3
2	1400	0.60	15.00	94.6
3	1000	1.00	15.00	95.6
4	1400	1.00	15.00	98.5
5	1000	0.80	10.00	96.3
6	1400	0.80	10.00	94.2
7	1000	0.80	20.00	92.3
8	1400	0.80	20.00	97.2
9	1200	0.60	10.00	93.5
10	1200	1.00	10.00	95.6
11	1200	0.60	20.00	93.8
12	1200	1.00	20.00	95.2
13	1200	0.80	15.00	96.5
14	1200	0.80	15.00	94.2
15	1200	0.80	15.00	95.6
16	1200	0.80	15.00	93.8
17	1200	0.80	15.00	94.8

It can be known from Table 8 that the experimental model is significant, which proves that the experimental design is reasonable and the data is valid. The p-value of the lack-of-fit term is 0.9891>0.05, indicating that the model has a high degree of fit and is relatively stable. The coefficient of determination of the model R^2=0.8667, and the regression equation has a good degree of fit. The rotation speed of the blade (A), the forward speed (B), the interaction term of the rotation speed of the blade and the forward speed (AB), the quadratic term of the forward speed (B^2), and the quadratic term of the diameter of the broad-leaved tall-stemmed plants stem (C^2) have a significant impact on the tip pruning efficiency, while the others are not significant. The influence-ability of each factor on the tip pruning efficiency is $B > A > C$.

Table 8 Variance analysis of the tip pruning rate of broad-leaved tall-stemmed plants stems

Source of variance	Sum of squares	Degree of freedom	Mean square deviation	F	p
Model	25.98	9	2.89	5.06	0.0220
A	4.96	1	4.96	8.69	0.0215*
B	6.48	1	6.48	11.35	0.0119*
C	0.011	1	0.011	0.020	0.8923
AB	4.20	1	4.20	7.36	0.0300*
AC	1.21	1	1.21	2.12	0.1887
BC	0.12	1	0.12	0.21	0.6572
A_2	0.056	1	0.056	0.098	0.7639
B_2	2.97	1	2.97	5.21	0.0565*
C_2	6.42	1	6.42	11.25	0.0122*
Residuals	4.00	7	0.57		
Term of lack of fit	0.11	3	0.036	0.037	0.9891
Pure error	3.89	4	0.97		
Total	29.98	16			

The experimental results are analyzed using the response surface methodology to obtain the influence of the interaction among different factors on the tip pruning efficiency, as shown in Figure 21.

Figure 21a shows the response surface plot of the influence of the blade rotation speed and the forward speed on the broad-leaved tall-stemmed plants stem tip pruning efficiency. As can be seen from the figure, when the forward speed remains constant, the broad-leaved tall-stemmed plants stem tip pruning efficiency first increases and then decreases with the increase of the blade rotation speed; when the blade rotation speed remains constant, the broad-leaved tall-stemmed plants stem tip pruning efficiency also first increases and then decreases with the increase of the forward speed. According to the change of the curved surface, it can be known that the blade rotation speed has a relatively significant influence on the broad-leaved tall-stemmed plants stem tip pruning efficiency.

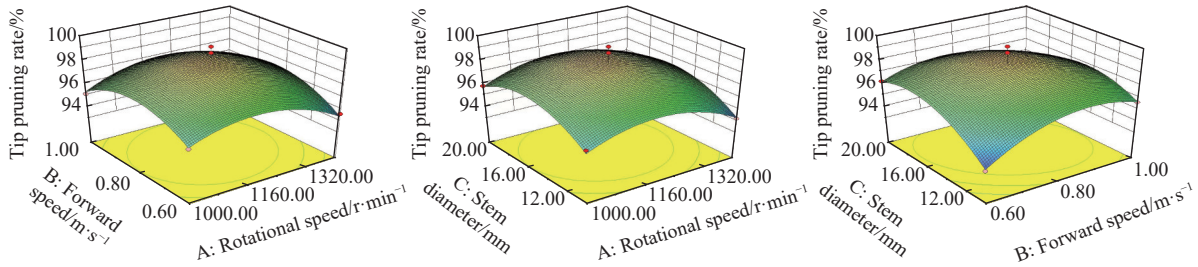

a. Response surface plot of tip pruning rate to forward speed and cutter rotational speed

b. Response surface plot of tip pruning rate to tobacco stem diameter and cutter rotational speed

c. Response surface plot of tip pruning rate to tobacco stem diameter and forward speed

Figure 21 Response surface of experimental factors on tip pruning efficiency

Figure 21b presents the response surface plot illustrating the impact of broad-leaved tall-stemmed plants stalk diameter and blade rotation speed on the tip pruning efficiency of broad-leaved tall-stemmed plants stalks. As can be observed from the plot, when the diameter of the broad-leaved tall-stemmed plants stalk remains constant, the tip pruning efficiency initially increases and then decreases with the increase in blade rotation speed. Conversely, when the blade rotation speed is held steady, the tip pruning efficiency first rises and subsequently falls as the broad-leaved tall-stemmed plants stalk diameter increases. The curvature of the surface indicates that the diameter of the broad-leaved tall-stemmed plants stalk has a more pronounced effect on the tip pruning efficiency.

Figure 21c is the response surface plot of the impact of the broad-leaved tall-stemmed plants stem diameter and the forward speed on the broad-leaved tall-stemmed plants stem tip pruning efficiency. As can be seen from the figure, when the forward speed remains constant, the broad-leaved tall-stemmed plants stem tip

pruning efficiency first increases and then decreases as the broad-leaved tall-stemmed plants stem diameter increases. When the broad-leaved tall-stemmed plants stem diameter remains constant, the broad-leaved tall-stemmed plants stem tip pruning efficiency first increases and then decreases as the forward speed increases. Based on the changes in the surface, it can be concluded that the broad-leaved tall-stemmed plants stem diameter has a relatively significant impact on the broad-leaved tall-stemmed plants stem tip pruning efficiency.

The analysis shows that when the optimal combination of the experimental factors is a forward speed of 0.8 m/s and a blade rotation speed of 1200 r/min, the tip pruning rate is 99.1%.

5 Verification test

In August 2024, a tip pruning experiment on potted broad-leaved tall-stemmed plants was conducted at the Yuanyang Branch of the Henan Academy of Agricultural Sciences. The main-cultivated variety "Qinyan-96" from Mianchi County, Sanmenxia was selected as the experimental object for the potted broad-leaved tall-stemmed plants. Before the experiment, a measuring tape was used to measure that the height of the broad-leaved tall-stemmed plants was 1.8-2.2 m, the height of the broad-leaved tall-stemmed plants flowers was 0.12-0.25 m[27,28], and the plant spacing was 0.5 m. The load platform used was a 10-kg plant-protection UAV designed and developed by Anyang Quanfeng Aviation Plant-Protection Technology Co., Ltd., and its flight speed was controlled at 0.5-1.0 m/s. The triangular-star-shaped broad-leaved tall-stemmed plants tip pruning device was processed by the Engineering Training Center of Henan Agricultural University. The experimental site is shown in Figure 22.

Figure 22 Experimental site

The tip pruning test method for broad-leaved tall-stemmed plants was carried out in accordance with the relevant production technical index regulations of the tip pruning operation in broad-leaved tall-stemmed plants field management. The test was divided into five repeated experiments in total. The number of broad-leaved tall-stemmed plants in each group was 10, and a grouped experiment was adopted. The calculation equation for the tip pruning rate is as follows:

$$Q = \frac{m}{M} \times 100\% \tag{20}$$

where, Q is tip pruning rate, %; m is the number of broad-leaved tall-stemmed plants for which the tip pruning test has been completed; and M is the total number of broad-leaved tall-stemmed plants in the tip pruning test.

As can be seen from Table 9, the test results are satisfactory. The effective tip pruning rate is 98.8%, and the operation efficiency is 0.2 hm²/h. The work efficiency is three times that of manual labor, which can meet the basic tip pruning requirements during the full-bloom period of broad-leaved tall-stemmed plants.

Table 9 Results of the tip pruning test

Test serial number	Total number of samples	Number of effective tip prunings	Tip pruning rate/%
1	100	98	98
2	100	100	100
3	100	98	98
4	100	99	99
5	100	99	99
Average	100	98.8	98.8

6 Conclusions

(1) This study proposes a blade-type broad-leaved tall-stemmed plants tip pruning test platform based on a low-load UAV. Through the star-type tip pruning cutter, diamond-shaped retractable mechanism, and adaptive control system, the transplanting mechanism realizes the autonomous locating and cutting of broad-leaved tall-stemmed plants flowers, which effectively solves the problems of broad-leaved tall-stemmed plants tip pruning operations.

(2) The dimensions and main mechanical properties of the broken part of the broad-leaved tall-stemmed plants top and the broad-leaved tall-stemmed plants top stem are measured by special experimental equipment. Based on the analysis and design software, the influence of each mechanism parameter on the flower-cutting performance was also analyzed. Optimal test data were obtained, which provides technical parameter support for the design and research of the UAV tip pruning mechanism.

(3) A comprehensive experimental study was carried out on the influence of the rotation speed of the tip pruning blade, the forward speed of the UAV during tip pruning, and the diameter of the broad-leaved tall-stemmed plants stem and flower part on the tip pruning efficiency. The results show that when the forward speed of the UAV is 0.8 m/s, the rotation speed of the broad-leaved tall-stemmed plants tip pruning blade is 1200 r/min. In addition, the diameter of the flowers during the full-bloom period is 15 mm, the tip pruning rate of this test bench is above 99.1%, and its operation performance is good, which can meet the actual production requirements.

(4) Due to the limitations of experimental conditions, potted plants were adopted for the verification test. There are certain differences in planting density, stalk toughness, and other aspects between potted and open-field crops, leading to the limitations of the test results. Field tests will be conducted in the later stage to improve the reliability of the test results.

Acknowledgements

This study is supported by the Key Research and Development Special Project of Henan Province (Grant No. 231111112800).

[References]

[1] Li J X, Li M Y, Zhao H, Zhu Q S, Gong S, Zhao S. Research progress on common diseases and pests of tobacco and their control measures in China. Modern Agricultural Science and Technology, 2024; 19: 68–72, 80. (in Chinese)

[2] Li X Y, Dong S Y, Zhang J H, Yang L. Research on key technologies in modern tobacco agricultural production. Full-text Edition of Chinese Science and Technology Journal Database (Agricultural Sciences), 2024; 10: 0086–0089. (in Chinese)

[3] Yu H Q, Huang C J, Yuan C, Zheng J M, Liu Y. Investigation of the types of mosaic virus diseases of flue-cured tobacco after tip pruning in Yunnan Province in 2020. Molecular Plant Breeding, 2024; 22(15): 5039–5046. (in Chinese)

[4] Han Y H, Liu C, Yang L, Yu T. Effects of tip pruning time and the number

of retained leaves on the growth and development of upper leaves of flue-cured tobacco in Shandong. Crops, 2023; 2: 157–162. (in Chinese)

[5] Ge J X, Zhang Q L, Cui Y J, Fu G Z, Wang X D, He J X. Effects of measures of increasing plant density and reducing the number of leaves on the growth, photosynthetic characteristics, yield and quality of flue-cured tobacco. Hubei Agricultural Sciences, 2024; 63(10): 68–73. (in Chinese)

[6] Liu Y F, Li H Y, Shan X H, Lei J, Yao Q, Ye W G, et al. Effects of tip pruning and auxin smearing on endogenous hormones and photosynthesis of upper leaves of flue-cured tobacco. Journal of Northwest A&F University (Natural Science Edition), 2021; 49(4): 47–54. (in Chinese)

[7] Zhang H C, Niu L L, Liu Y. Discussion on the strategies for high-quality development of modern tobacco agriculture. Full-text Edition of Chinese Science and Technology Journal Database (Natural Sciences), 2024; 11: 082–086. (in Chinese)

[8] Dong S S. An analysis of the relationship between modern agricultural mechanization and agricultural planting technology. Southern Agricultural Machinery, 2024; 55(16): 84–86. (in Chinese)

[9] Li J. Current situation, problems and countermeasures of tobacco agricultural mechanization. Full-text Edition of Chinese Science and Technology Journal Database (Agricultural Sciences), 2024; 5: 0033–0036. (in Chinese)

[10] Liu C, Li J Z, Wang H B, Peng Z G, Duan M Z, He W. Analysis of the development status and countermeasures of mechanical tobacco leaf harvesting. Southern Agricultural Machinery, 2024; 55(10): 24–28, 32. (in Chinese)

[11] Li J Y, Zhang D, Yin G Y, Li Y H, Zhang F S, Liu J J, et al. Thoughts on the integrated development of tobacco agricultural machinery and agronomy in the northern plain areas: taking the tobacco leaf production areas in Pingdingshan City as an example. Agricultural Engineering, 2024; 14(6): 15–19. (in Chinese)

[12] Wu Z N, Rong M M, Li W, et al. Research progress of tobacco tip pruning and sprouting suppression machine. Hebei Agricultural Machinery, 2023; 11: 13–15. (in Chinese)

[13] Liu Y, Niu L L, Wu J, Liu L, Cheng Y Y, Li L H, et al. Design of the collection device for tobacco tip pruning and bud suppression. Agricultural Equipment & Vehicle Engineering, 2024; 62(5): 23–27. (in Chinese)

[14] Han X, Han J G, Chen Y L, Lan Y B, Li J K, Cui L H. Research on the cotton chemical tip pruning system based on intelligent identification of apical buds. Transactions of the CSAM, 2024; 55(3): 145–152. (in Chinese)

[15] He H, Sun Y G, Shi Y K, Wang Y H, Zhao Q M, Xie Q, et al. Study on plant type characteristics of tobacco varieties suitable for mechanical tip pruning. Chinese Tobacco Science, 2025; 46(4): 1–8. (in Chinese)

[16] Han S, Liu Y, Wu J, Li Q, Liu L, Li L H, et al. Preliminary study on the mechanical properties of bending and tensile of tobacco stems. Farm Machinery Use & Maintenance, 2024; 1: 1–4, 9. (in Chinese)

[17] Yang H W, Zhang L Y, Tang Z Q, Yu F H, Xu T Y. Effects of mechanical traits and physicochemical characteristics of stems of hybrid japonica rice on lodging resistance. Transactions of the CSAE, 2024; 40(14): 44–52. (in Chinese)

[18] Li L F. Design and experiment of scraper-type integrated machine for tobacco tip pruning and suckering. Northwest A&F University, Yangling, China, 2024. DOI: 10.27409/d.cnki.gxbnu.2024.002384 (in Chinese)

[19] Handayani D, Okhuysen V F, Wagner N. Machinability of high Mn steel using tool life criteria. International Journal of Metalcasting, 2023; 17(2): 456–468.

[20] Yan C G, Yu J B, Jia G G, Xu L. Experimental study on tool life in milling ZGMn13 high manganese steel. Tool Engineering, 2009; 43(5): 21–24. (in Chinese)

[21] Hu Y N, Wang C Y, Ding H N. The mechanical performance of diamond saw blades with special structure. Advances in Grinding and Abrasive Processes, 2004; 259(2): 141–145.

[22] Li L H, Li J Y, Sun W X, Sun Q T, Qin W H, Ma G Z, et al. Design and experiment of saw blade type tobacco tip pruning device based on UAV load platform. Journal of Agricultural Mechanization Research, 2026; 1: 1–7. (in Chinese)

[23] Ren Z. Kinematic simulation analysis of an elderly-assisting lifting device based on ADAMS. Mechanical Research & Application, 2023; 36(5): 6–8. (in Chinese)

[24] Zhou G G, Sun J X, Wang B, Lei H Z, Huang H, Fan H X, et al. Design of silkworm cocoon picking mechanical system based on ADAMS. International Journal of Plant Engineering and Management, 2024; 29(2): 97–114.

[25] Yang Z, Yang X, Yang X B, Wang P F, Li J P, Liu H J, et al. Parameter optimization design of the cutter of apple seedling stump planter based on virtual orthogonal test. Journal of Agricultural Science and Technology, China, 2021; 23(1): 98–106. (in Chinese)

[26] Guo X A, Mao Z Y, Shi Z D, Lu W. Lightweight and high-security laser-based cotton tip pruning robot. International Journal of Agricultural and Biological Engineering, 2024; 17(4): 98–108.

[27] Shao X L, Yang M, Zhang R Y, Wang X J, Xu W. Application of good agricultural practice in tobacco planting. Modern Agricultural Science and Technology, 2011; 15: 97–98. (in Chinese)

[28] Sheng H H. An analysis of the key points of tobacco planting and field management techniques. Jiangxi Agriculture, 2024; 7: 55–57. (in Chinese)